International Journal of Pharmaceutics 657 (2024) 124174

Contents lists available at ScienceDirect

International Journal of Pharmaceutics

journal homepage: www.elsevier.com/locate/ijpharm

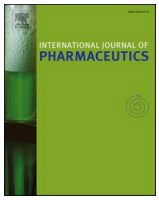

UV imaging for the rapid at-line content determination of different colourless APIs in their tablets with artificial neural networks

Máté Ficzere [a], Lilla Alexandra Mészáros [a], Anna Diószegi [a], Zoltán Bánrévi [a], Attila Farkas [a], Sándor Lenk [b], Dorián László Galata [a], Zsombor Kristóf Nagy [a,*]

[a] Department of Organic Chemistry and Technology, Faculty of Chemical Technology and Biotechnology, Budapest University of Technology and Economics, Műegyetem rkp 3., H-1111 Budapest, Hungary
[b] Department of Atomic Physics, Budapest University of Technology and Economics, Műegyetem rkp 3., H-1111 Budapest, Hungary

ARTICLE INFO

Keywords:
UV imaging
API content measurement
Artificial neural network
Process analytical technology
Machine vision
Tableting
Quality assurance

ABSTRACT

This paper presents a novel high-resolution and rapid (50 ms) UV imaging system, which was used for at-line, non-destructive API content determination of tablets. For the experiments, amlodipine and valsartan were selected as two colourless APIs with different UV induced fluorescent properties according to the measured solid fluorescent spectra. Images were captured with a LED-based UV illumination (385–395 nm) of tablets containing amlodipine or valsartan and common tableting excipients. Blue or green colour components from the RGB colour space were extracted from the images and used as an input dataset to execute API content prediction with artificial neural networks. The traditional destructive, solution-based transmission UV measurement was applied as reference method. After the optimization of the number of hidden layer neurons it was found that the relative error of the content prediction was 4.41 % and 3.98 % in the case of amlodipine and valsartan containing tablets respectively. The results open the possibility to use the proposed UV imaging-based system as a rapid, in-line tool for 100 % API content screening in order to greatly improve pharmaceutical quality control and process understanding.

1. Introduction

In the pharmaceutical industry, the currently widespread Quality-by-testing (QbT) approach is applied as quality control strategy during production, where small samples undergo slow, destructive, off-line laboratory testing (Nagy et al., 2022; Yu, 2008). If the evaluated quality parameters meet the specifications, the product is available for release, if not, the entire batch could be discarded, resulting in severe financial loss (Rossi, 2022). To combat this phenomenon and to better understand the steps of pharmaceutical manufacturing the concept of process analytical technology (PAT) was introduced. This initiative is greatly supported by the regulatory authorities (Food and Drug Administration, 2004) and has also attracted the interest of pharmaceutical manufacturers. These tools possess the capability to enhance the comprehensive understanding of the processes and the product, as well as rapidly analyze and control any deviations from specifications that may arise during production (Casian et al., 2022).

Considering the Quality-by-design (QbD) approach, the content and the content uniformity of the active pharmaceutical ingredient (API) are regarded as high-risk critical quality attributes (CQAs) (Kandpal et al., 2017). Recalls have been initiated by the authorities related to the mentioned attributes, which emphasize the significance of these concerns (Food and Drug Administration, 2024). Therefore, multiple faster methods were developed to replace the traditional destructive, off-line measurements. Several publications in the literature showcase that near infrared (NIR) and Raman spectroscopy surfaced as suitable PAT tools for the API content determination of tablets. NIRS has already been used as to predict API content of tablets manufactured at various levels of compression force (De Man et al., 2023), to assess API content and tablet hardness (Kandpal et al., 2017), and to compare the concentration of API in a tablet press feed frame and in tablets (Peeters et al., 2022). Transmission Raman spectroscopy has also been applied to assess the content uniformity of tablets as a standalone method (Belay et al., 2021) or coupled with NIRS (Wang et al., 2021). However, these spectroscopic methods have a high investment cost, and they also yield complex data that can be difficult to interpret.

* Corresponding author.
E-mail address: zsknagy@oct.bme.hu (Z. Kristóf Nagy).

https://doi.org/10.1016/j.ijpharm.2024.124174
Received 14 March 2024; Received in revised form 17 April 2024; Accepted 26 April 2024
Available online 1 May 2024

Artificial neural networks (ANNs), which have improved dramatically in the last few years, are capable of handling of such complex datasets, with non-linear correlations as inputs (Das and Chakraborty, 2016; Djuris et al., 2021). This advanced multivariate data analysis method is widely applied to perform regression or classification tasks (Butts et al., 2003), especially when coupled with NIRS (Péterfi et al., 2023). Several publications can be found in the field of *in vitro* dissolution predictions of various tablets with ANNs (Baranwal et al., 2019; Galata et al., 2021a; Nagy et al., 2019). Neural networks can also be used to efficiently and accurately analyse data gathered from other inputs, such as machine vision systems.

Machine vision can be used as an innovative analytical method in the field of pharmaceutical manufacturing with several advantages, such as its fast data acquisition and low investment cost. By utilizing RGB cameras, the concentration of different coloured components can be monitored during various steps of the manufacturing process (Galata et al., 2021c). There have been cases reported, where the content of riboflavin, a yellow-coloured API was determined using machine vision during continuous blending and continuous twin-screw wet granulation even at a concentration of 0.05 w/w% (Ficzere et al., 2021; Galata et al., 2021b). In addition to the widespread usage in the case of powders, tablets containing coloured components could also be investigated with machine vision (Wagner et al., 2000; Wagner et al., 1999). These methods all utilized visible illumination, which however can only be used in the case of coloured APIs for direct concentration measurement.

UV imaging is a novel, fast and non-destructive tablet inspection method, which is attracting substantial interest. Wu et al. successfully applied multispectral UV imaging at six different wavelengths for the visualization of glibenclamide in tablets (Wu et al., 2014). The same approach was applied later for the non-destructive determination of tablet physical properties and for pellet visualization in tablets (Klukkert et al., 2016; Novikova et al., 2016). However, in all of these cases, due to the consecutive manner of data acquisition at different wavelengths, the acquisition time was 18 s per multispectral image. This long measurement time limits the number of samples, thus making multispectral UV imaging in a consecutive manner not suitable for real-time monitoring.

By exposing a tablet only to a single wavelength of UV light, its components can turn into different colours due to slight differences in absorption or fluorescence. This can be used to predict the API content and particle size distribution, and also the dissolution profile of the tablets at much higher speed and combined with an RGB camera, the resolution is greatly increased as well (Mészáros et al., 2022). In a previous work (Mészáros et al., 2020) of the authors, single wavelength UV/VIS imaging was utilized to measure the drug content, dissolution profile and crushing strength of tablets containing a yellow model drug, meloxicam. For API content determination, the applied acquisition time was 1.2 ms, which is four magnitudes faster than in the case of multispectral UV imaging. With RGB and CIELAB colour space-based algorithms they could predict the API content of the tablets with a relative error of 4.9 %. However, there have been no cases reported where tablets containing APIs that are colourless in visible light were investigated using fast, single wavelength UV imaging for API content determination.

The aim of our study is to utilize a UV imaging-based machine vision system as a novel PAT tool for the fast and accurate concentration determination of colourless APIs in white tablets. We intend to use two, antihypertensive APIs that have different fluorescent properties to showcase the wide applicability of UV imaging. Amlodipine functioned as a highly UV fluorescent, while valsartan was a non-UV fluorescent API at the applied wavelength. These model APIs also vary in particle size, thus we also aim to analyse the effect of this attribute on the prediction of API content. The applied excipient matrices also model the composition of products currently available on the market (Sandoz Group AG, 2018; Teva, 2022). We aim to utilize ANNs for the determination of API content, creating a fast, non-destructive machine vision-based method that could be used as a part of a real-time monitoring system.

2. Materials and methods

2.1. Materials

The model APIs amlodipine and valsartan were obtained from Sigma-Aldrich (St. Louis, Missouri, USA). These are frequently applied either separately or in a combination. Microcrystalline cellulose (MCC) and calcium hydrogen phosphate (CHP) were both purchased from JRS Pharma (Rosenberg, Germany). Magnesium stearate was acquired from Hungaropharma Ltd. (Budapest, Hungary) and corn starch was obtained from Merck (Budapest, Hungary).

2.2. Methods

2.2.1. Preparation of tablets

For the experiments two sets of biconvex tablets with a target weight of 400 ± 20 mg were produced on a Dott Bonapace CPR-6 (Limbiate, Italy) single punch tablet press, using concave punches with a diameter of 14 mm and the compression force was set to 14 kN. To model a commercially available formulation with a target API content of 2.5 mg, 7 groups of low dose amlodipine tablets were produced consisting of 9–9 tablets containing 187.25 mg CHP, 20 mg corn starch and 2 mg magnesium stearate. The amlodipine content was different in each group, set to the values presented in Table 1 and the MCC content was altered accordingly. In total 63 tablets were produced containing the mentioned API. Valsartan tablets contained the commercially available doses shown in Table 1 and the rest of them consisted of MCC. A total number of 64 valsartan tablets were manufactured. The target dose was determined by the authors as 60 mg.

2.2.2. UV image and fluorescent spectra acquisition

Image acquisition was carried out using a Canon 650D (Canon, Tokyo, Japan) digital single-lens reflex (DSLR) camera equipped with a Canon EFS 18–55 macro lens (Canon, Tokyo, Japan) mounted using a reversing ring. UV illumination was provided by a ring light (Apokromat Ltd, Budapest, Hungary) which contained a single row of light-emitting diodes (LED) with an emission spectral range of 380–395 nm. The implemented system is operating in reflection mode. A dark box was used to exclude the outside light. Exposure time was set to 1/20 s. Images were captured from both sides of the tablets with a resolution of 5184 × 3456 pixels. Between the camera and the computer, an USB 3.0 interface provided the connection. The setup is similar to the one used in a previous work of the authors (Mészáros et al., 2020). VIS images were acquired for the visual comparison of the samples using the mentioned set up with a ring light, containing 3 rows of LEDs in the emission range of VIS.

The fluorescent spectroscopy measurements were carried out using an RF-6000 spectrofluorometer (Shimadzu Corporation, Kyoto, Japan) with an excitation wavelength of 385 nm with slit bandwidths of 5 nm for both excitation and emission, and a scan speed of 200 nm/min. For the measurements, solid samples of pure amlodipine and valsartan were cold-pressed into a disk with a thickness of 10 mm. The fluorescent emission was detected from 400 nm to 700 nm.

Table 1
The amlodipine and valsartan content of each sample group.

API content of amlodipine tablet groups [mg]	API content of valsartan tablet groups [mg]
1.75	20
2.00	40
2.25	80
2.50	160
2.75	
3.00	
3.25	

2.2.3. Measurement of API content with UV/VIS spectrometry

The validation of the API content predictions was carried out with UV absorption spectroscopy using flask method. An Agilent 8453 UV/VIS spectrometer (Hewlett-Packard, Palo Alto, CA, USA) was used for the API content measurements. The amlodipine content determination was done by dissolving the tablets in 200 mL volumetric flasks using 200 rpm stirring for 3 h in distilled water. Then the solutions were filtered using a 1.2 μm syringe filter (Labex Ltd, Budapest, Hungary). The amlodipine content was measured at 242 nm with a 10 mm cuvette. For the measurement of valsartan, the tablets were dissolved in 6.8 pH phosphate buffer and the measurements were taken at 252 nm in a 10 mm cuvette.

2.2.4. Determination of API content with artificial neural networks

In order to predict the API content of the produced tablets, the acquired images were analysed with an algorithm developed in Matlab 9.12.0.2327980 (Mathworks, Natick, MA, USA) environment. For the ANN-based prediction Matlab Deep Learning toolbox 14.0 (Mathworks, Natick, MA, USA) was applied. Fig. 1 presents a flowchart of the applied algorithm. The first step of the image processing was the background extraction. With the application of B (blue) values of the pixels, binarization was carried out enabling the Hough-transformation based circle detection with a set range of radii of the samples.

For the evaluation of amlodipine containing samples RGB colour space was applied. From the extracted colour components, the B channel was used in the following steps. Histograms were created from the mentioned values of the pixels for both sides of the tablets, which were then averaged. These were used to create the input dataset for the ANN. The training set contained 52 samples and the test set consisted of 11 samples, which means that 83 % and 17 % of the samples were utilized in the datasets. A classic feed-forward structure was chosen, with input, hidden and output layers, one from each. Bayesian regularization backpropagation was used as a training function. In the case of a small dataset this function can successfully avoid overfitting. In the optimization process the number of neurons used in the hidden layer was altered between 1 and 5. The training was carried out for maximum 40 epochs. The early stopping of the training is also applied to reduce the occurrence of overfitting. The hyperparameters of the ANN were set to default. The optimal neuron number was chosen by comparing the average RMSE (root mean square error) values for the training and test set, each calculated by the following equation:

$$RMSE = \sqrt{\frac{\sum_{i=1}^{n} \left(y_{predicted} - y_{measured}\right)^2}{n}} \quad (1)$$

where n is the number of samples, $y_{predicted}$ is the API content value obtained with UV imaging and $y_{measured}$ is the API content measured with UV/VIS spectrometry. The ensemble of 50 trained ANNs employing the optimal number of neurons, was utilized to execute the prediction of the content. The individual results of the ANNs were averaged. This approach can effectively mitigate overfitting, reduce prediction variability, and enhance model generalization capabilities.

RGB colour space was also used for the evaluation of valsartan containing samples. After the colour component extraction, the G (green) channel was used in the following steps. Histograms were created from the mentioned values, and these were used to create the input dataset for the ANN. The training set contained 52 samples and the test set consisted of 12 samples, which means that 81 % and 19 % of the samples were utilized in the datasets. The above-mentioned ANN structure and training function were also applied in this case. In the optimization process the number of neurons used in the hidden layer was also altered between 1 and 5. In comparison to amlodipine, the task's complexity is reduced mainly because it involves only four API content levels. Furthermore, the significant differences observed in the histograms may require different numbers of epochs to adequately capture the underlying correlations. This can lead to faster convergence to the optimum when compared to the scenario involving amlodipine, resulting in that the training process was carried out for maximum 15 epochs. The optimal neuron number was also chosen by comparing the average RMSEP values obtained for the training and test sets.

3. Results and discussion

3.1. Physical characterization of the produced tablets

For the characterization studies, amlodipine and valsartan tablets were randomly selected, and their individual mass (n = 20), tensile strength (n = 10, Dr. Schleuniger THP-4 M tablet hardness tester; Dr. Schleuniger Productronic, Solothurn, Switzerland) and friability (n = 10, PTF E double drum friability tester; Pharma Test Apparatebau AG, Hainburg, Germany) were evaluated. Table 2 presents the results of the characterization.

Based on these results it can be concluded, that the produced tablets meet the Ph. Eur. criteria on uniformity of individual mass (European Pharmacopoeia Commission, 2019b) and friability (European Pharmacopoeia Commission, 2019a). The tensile strength values indicate that the tablets were indeed manufactured with the same level of compression force, resulting in a similar surface texture for the tablets. Therefore, the was no need to include a parameter regarding surface roughness into the models.

3.2. Fluorescent properties of amlodipine and valsartan tablets

To assess the range of applicability of the UV imaging-based machine vision system, the authors have chosen two APIs with distinct fluorescent characteristics. Based on the registered fluorescence emission spectra at the excitation wavelength of 385 nm (presented on Fig. 2), amlodipine is an intensively fluorescent molecule with a peak at 451 nm,

Table 2
The physical characteristics of the tablets, where RSD is the relative standard deviation and SD is the standard deviation.

Individual mass [mg] (n = 20, mean ± SD)	RSD [%]	Tensile strength [N] (n = 10, mean ± SD)	Friability [%] (n = 10)
400.64 ± 5.742	1.43	130.2 ± 6.29	0.49

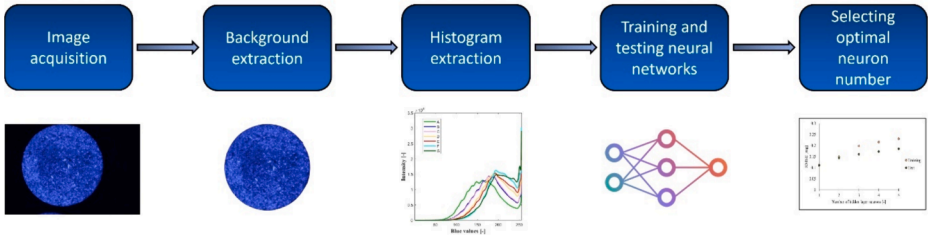

Fig. 1. Flowchart of the algorithm.

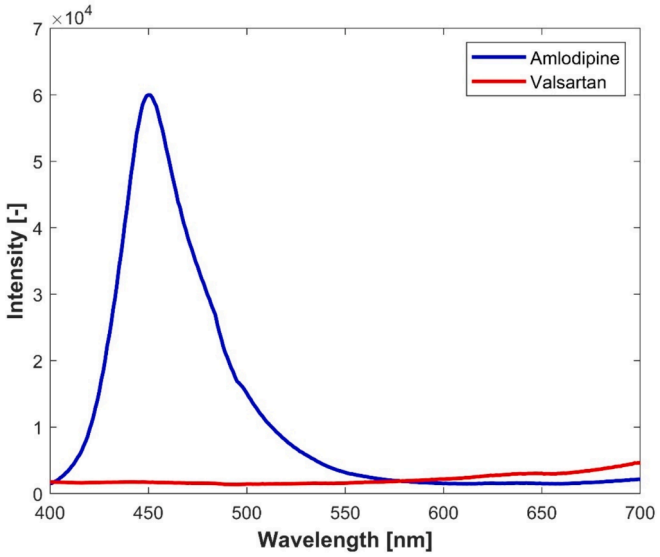

Fig. 2. Fluorescent spectra of amlodipine and valsartan at the excitation wavelength of 385 nm.

while valsartan is a non-fluorescent API.

Based on the results, differences in the appearance of amlodipine and valsartan containing tablets under UV illumination are expected. Fig. 3 presents a comparison between the surface of an amlodipine and a valsartan tablet on images taken with the machine vision system using VIS and UV illumination.

As observed by visual inspection, in neither case is the API distinguishable on the surface of white tablets under VIS illumination. Consequently, the API content may not be measured using that illumination spectral range. On the other hand, applying UV range illumination makes both the APIs and excipient particles visible to the naked eye due to fluorescence contrast between the components. This also allows the possibility of differentiating the matrix elements and the API using the colour components, while also enabling the qualitative particle size determination of the APIs.

The visualization of the changes in the surface related to the increasing API content is shown on Fig. 4 for amlodipine and Fig. 5 for valsartan containing samples. As a highly UV- fluorescent API in the applied range (Fig. 2), amlodipine has a bright hue in the blue component on the UV illuminated images, which overshines the darker colour of all the other excipients in the tablet. However, the midtones and the dark tones of the blue component can also be used to differentiate between the applied matrix components. Moreover, it can be seen on Fig. 4 that the surface of tablets containing more API particles with increasing API content levels, thus increasing the overall brightness, while the colour of the matrix components is more supressed.

Valsartan, as a non-UV fluorescent component (Fig. 2), has a darker blue hue, while the excipient has brighter shades, resulting in different detectable regions on the surface for the naked eye. Fig. 5 shows that tablets containing a higher amount of valsartan exhibit deeper blue hue. Because of the smaller particle size of this API, only a few bigger particles are distinguishable by the naked eye, but the presence of smaller particles can be detected in the shift of the hue as the content increases. It is also important to note that between the smallest and the largest levels of content there is significant difference in the hue, however between the 20 and 40 mg levels this can be slightly observed by the naked eye. To conclude, this shift in colour occurring due to the increasing API content may provide an opportunity to evaluate the mentioned CQA.

The mentioned observations correlate with the fluorescent spectroscopy measurements (Fig. 2) and made the qualitative analysis of the

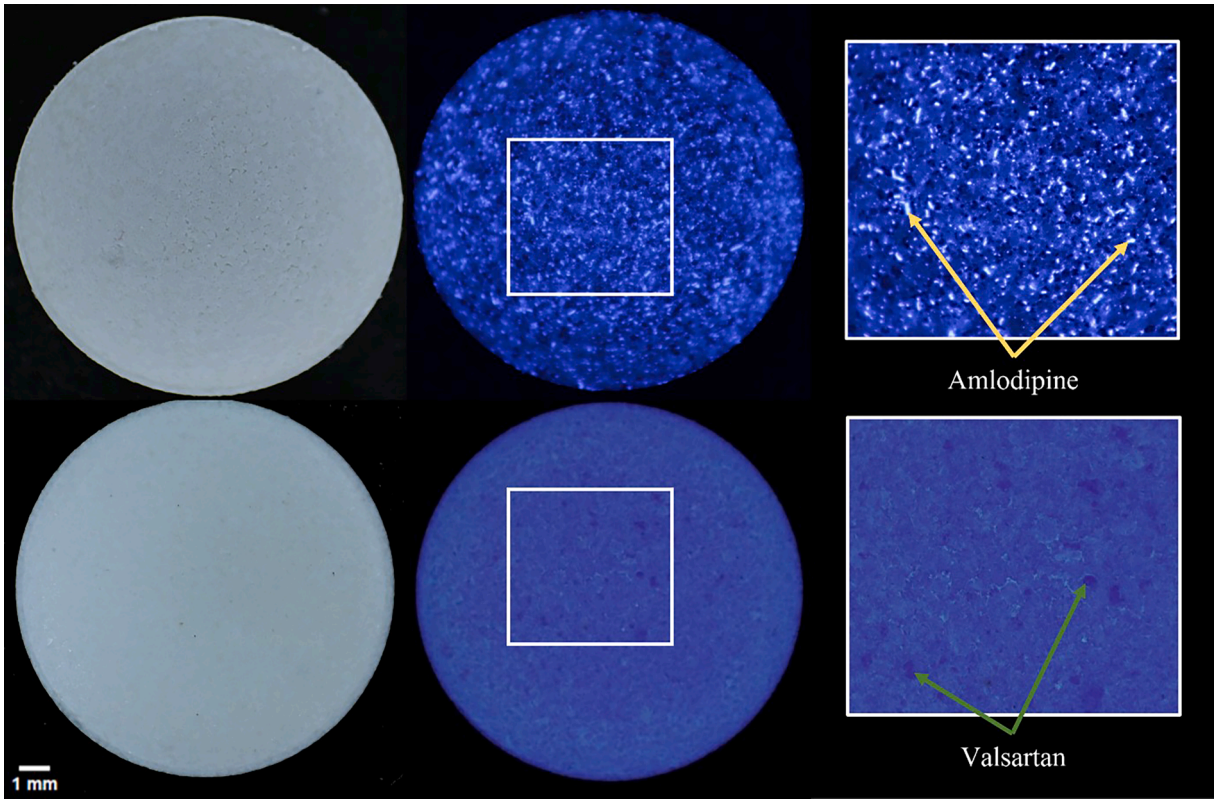

Fig. 3. The first column displays images of tablets illuminated with VIS, while the second column shows the same tablets illuminated with UV. The third column features an enlarged section of the sample surface, with arrows indicating the API particles. The top row consists of amlodipine tablets, while the second row shows valsartan tablets.

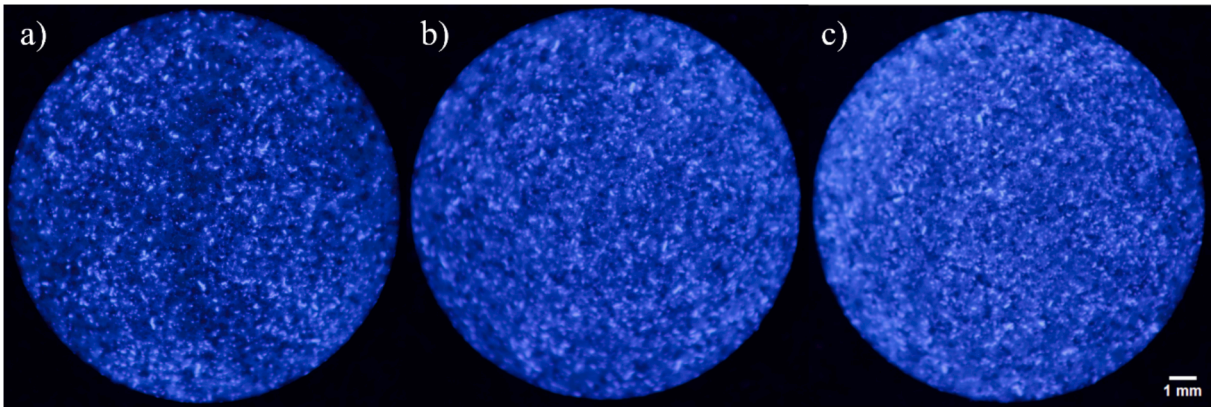

Fig. 4. UV images of amlodipine containing tablets with a nominal dose of 1.75 mg (a), 2.5 mg (b), and 3.25 mg (c).

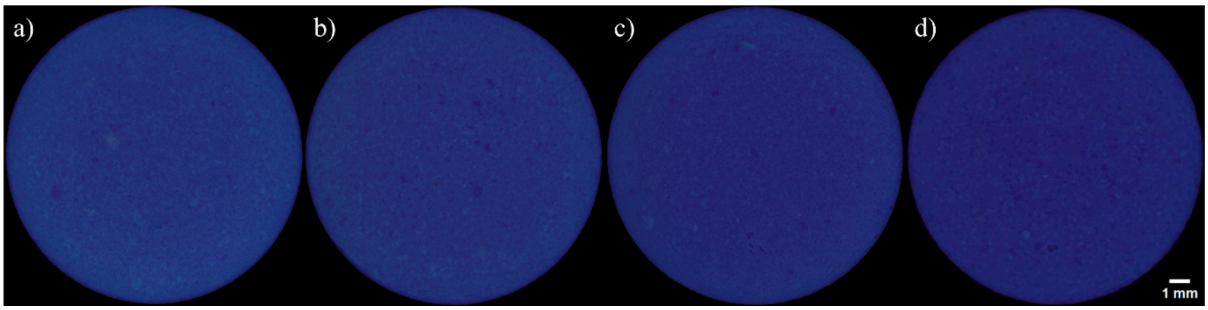

Fig. 5. UV images of valsartan containing tablets with a nominal dose of 20 mg (a), 40 mg (b), 80 mg (c), 160 mg (d).

tablet components possible, but to enable quantitative analysis, tablets containing different amounts of APIs should be investigated.

3.3. *Preparing the input dataset for the development of the ANN model*

In order to create the input dataset for the ANNs, histograms were constructed of images taken of both sides of the samples produced for the experiments. The histograms were averaged for each group of tablets with the same dosage and shown in Fig. 6 *a)* for amlodipine and Fig. 6 *b*) for valsartan tablets.

By investigating the average histograms of amlodipine tablets (Fig. 6 *a)*), it can be seen that the higher doses have higher intensity in B values. The histograms correspond with the earlier perception that tablets with a higher amlodipine content have brighter colour due to the increasing number of API particles on the surface. The presence of this trend is particularly noticeable, within the range of 200–255. Furthermore, in the case of smaller doses, the smaller number of particles and the darker colours of the excipients become visible, shifting the histograms to the left. Consequently, the whole range of the histogram should be analysed to obtain the proper information for the analysis. The utilization of histograms enables the extraction of diverse information from the samples, thereby facilitating the applicability of multivariate data analysis methods, such as ANNs. In conclusion a strong correlation can be observed between the B histograms of the samples and the applied dosage levels, enabling the usage of histograms as a proper input for API content prediction.

The average G histograms of valsartan tablets (Fig. 6 *b)*) also show a clear separation of the dosage groups. Samples containing more API

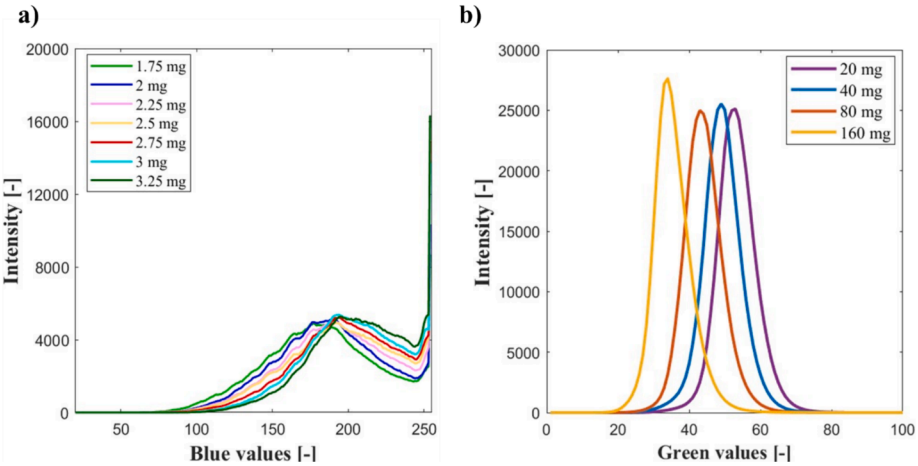

Fig. 6. The average B histograms of the amlodipine (a) and the average G histograms (b) of valsartan tablets for each dosage group.

have lower G values, therefore they are darker, corresponding with the previous observations. In the context of these histograms, the peaks shifted towards the lower values with increasing API content. Compared to the histograms of amlodipine, a narrower distribution of the values can be observed, which can be explained by the small changes of the hue throughout the increasing dosage levels. It is important to mention that, despite the fact that the changes can also be observed in the blue component, the hue change is found to be more differentiative in the green component. To conclude, the investigation of the histograms showed that they are suitable for presenting the differences between the different dosage groups, making them preferable as input data for ANNs.

3.4. Development and optimization process of the ANN-based models

3.4.1. ANN-based model for the prediction of amlodipine content

Model development

The UV imaging-based input dataset was used to determine the API content of the tablets with ANNs. In the case of amlodipine tablets, a total of 63 tablets were split into training and test groups at random, which contained 52 and 11 tablets respectively. In order to select the optimal number of hidden layer neurons, 50 ANNs trained with 1 to 5 neurons. The RMSE values were compared using boxplots (Fig. 7 *a)* and *b)*). The comparison of the obtained averaged RMSE values for the training and test set of samples are presented on Fig. 7 *c)*.

As it can be observed, the number of hidden layer neurons greatly impacts the RMSE values. By increasing the neuron number, the training and test RMSE values both increase, indicating a less accurate model. Furthermore, the gap between the training and test RMSE values is growing as well, which results the occurrence of overfitting. It is worth noting that increasing the number of neurons in the hidden layer also significantly increases the training time of the ANN. In order to acquire a robust model with the applied training set consisting of a relatively small number of samples, 1 or 2 neurons should be used in the hidden layer, based on the RMSE values. On the other hand, with two neurons in the hidden layer the standard deviation of the 50 training cycles is obtained at higher levels. Based on the low-level of complexity of the input dataset it is expected to obtain a model that is not prone to overfitting with a simple ANN structure and a small number of neurons in the hidden layer. Considering all observations, 1 hidden layer neuron was selected as the best option and was used in the following for amlodipine content prediction.

In the context of the goodness parameters of the structurally simple, optimized ANN the averaged RMSE values are 0.111 mg for the training set and 0.112 mg for the test set. It meant 4.4 % of relative error on the target value of 2.5 mg, which is in the range of the ± 5 % limit for the API content determination (Casian et al., 2017). In conclusion, the acquired images and the colour component histograms, such as B values of the samples can become valuable information sources when the formulation contains a highly UV fluorescent substance as an API.

Evaluation the results obtained for the test set of the ANN-based prediction of amlodipine content

Fig. 8 showcases the predicted and the measured amlodipine contents of the test set. When the trends in the measured and predicted values are compared, it can be observed that the prediction follows the trend obtained from the measurements. Moreover, the predicted values are close to the measured contents.

Table 3 shows the detailed comparison of the measured and the predicted, averaged values with the trained 50 ANNs using one neuron in the hidden layer. The calculated relative errors are also presented for the samples of the test set. As showcased, the amlodipine content of the tablets was determined without systematic error and with high accuracy. Larger deviation from the measured value is obtained at the 2nd, 5th and 9th samples. However, these error values are in the range of the ± 10 % limit. In all the other cases the relative error is under 5 %, averaging 4.41 %. Nevertheless, increasing the number of samples could enhance the accuracy of the ANN model.

In conclusion the developed, simple image processing method was capable of extracting the appropriate information from the images in the

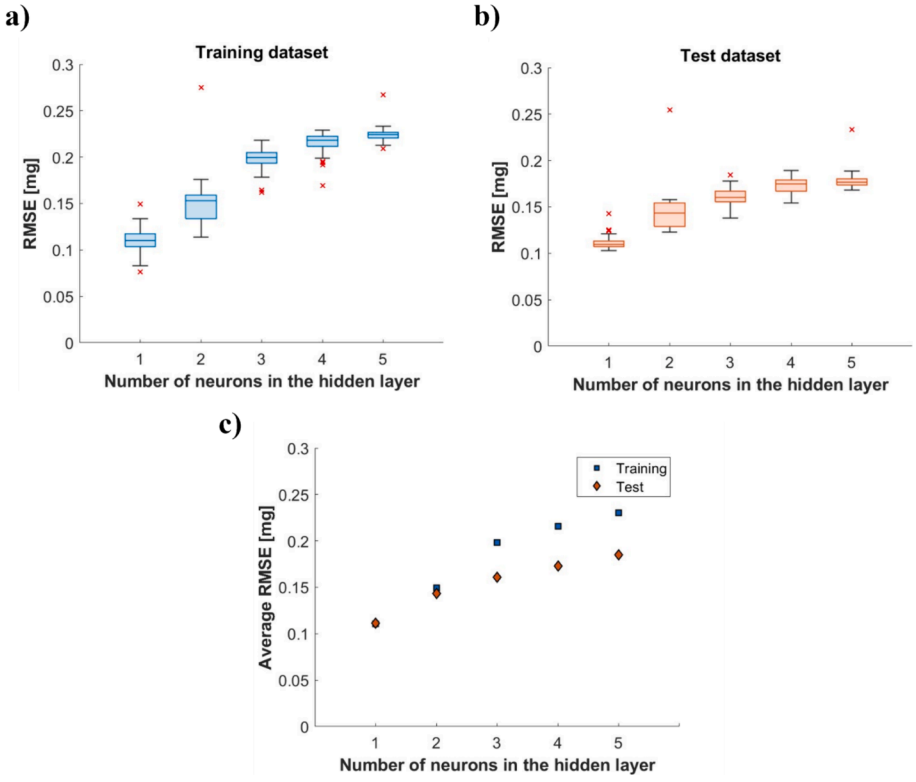

Fig. 7. The results of the optimization process of the ANN-based model for the training (a) and test set (b) of amlodipine content prediction with different numbers of neurons in the hidden layer, and the trend obtained in the averaged RMSE values (c).

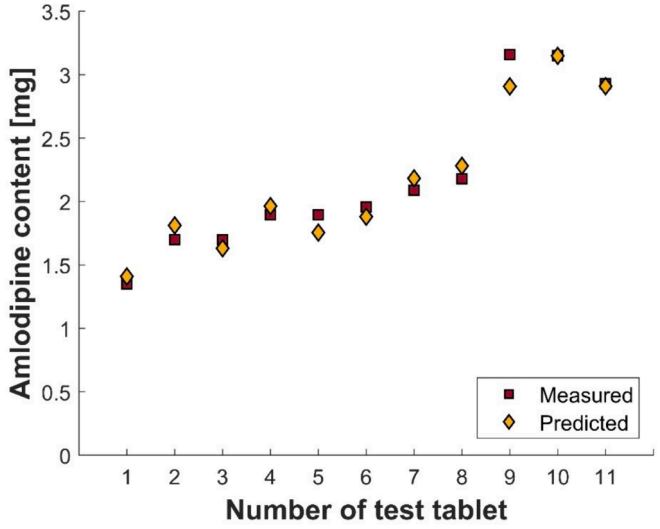

Fig. 8. The amlodipine content of the test tablets predicted with the optimized ANN-based model and measured using standard method of UV spectrometry.

Table 3
Predicted and measured amlodipine content of the test set and the relative error values for each sample.

Number of test tablet [-]	Amlodipine content predicted with ANN [mg]	Amlodipine content measured with UV spectrometry [mg]	Relative error of prediction [%]
1	1.41	1.35	4.35
2	1.81	1.70	6.61
3	1.63	1.70	−3.99
4	1.96	1.90	3.57
5	1.76	1.89	−7.36
6	1.88	1.96	−3.98
7	2.18	2.09	4.54
8	2.28	2.18	4.65
9	2.91	3.16	−7.95
10	3.15	3.15	−0.09
11	2.91	2.93	−0.70

context of a highly UV-fluorescent API. Only by utilizing UV illumination is an opportunity provided, where white amlodipine particles become visible on the surface of the samples. The changes in the histograms of B values showed strong correlation with the changes in the content of amlodipine, thus it was sufficient for the training of an ANN with a simple structure. The larger size of the API was not a limiting factor in the context of image processing or prediction. As presented, the amlodipine content of the tablets was determined without systematic error and with high accuracy. The average relative error of the prediction is 4.41 %, which is a very suitable result for a novel rapid machine vision method with a measurement time of only 50 ms, making it a promising tool for future applications.

3.4.2. *ANN-based model for the prediction of valsartan content*

Model development

To explore the range of applicability of the UV imaging system, valsartan was applied as a non-fluorescent API, due to its different appearance on the tablet surface in comparison with amlodipine containing samples. In that case, a total of 64 tablets were randomly split into training and test groups containing 52 and 12 tablets. In order to determine the optimal number of hidden layer neurons, like previously, the RMSE values were calculated from 50 training cycles and visualized on boxplots (Fig. 9 *a) and b)*). The averaged RMSE values were compared in Fig. 9 *c)*.

It was observable, just as in the case of the amlodipine containing samples, the number of hidden layer neurons significantly influences the training and test RMSE values, thus the performance of the ANNs. The test RMSE values at higher neuron numbers are larger than the training values, which can indicate overfitting. Due to the low complexity of the input dataset, ANNs with 1 hidden layer neuron yielded the best performance and were used for the valsartan content prediction. Based on the differences in the G histograms and the levels of the API content the standard deviations were small both for the training and test sets as expected. The obtained RMSE for the training set was 2.54 mg and for the test set this value was 2.70 mg. By applying a simple network structure, the ANN is also less prone to overfitting.

To summarize the results obtained throughout the optimization process, the machine vision-based dataset was also applicable for the training of the ANN and for the prediction of the non-fluorescent API content. Moreover, the darker colour and the smaller particle size of the API are not limiting factors in the context of the prediction of the valsartan content.

Evaluation the results obtained for the test set of the ANN-based prediction of valsartan content

Fig. 10 illustrates the valsartan contents of the test set of samples, both predicted and measured. Just as the prediction of amlodipine content, the predicted values show a trend consistent with the measured values. Additionally, the estimated content values closely approximated the values determined using UV spectroscopic method.

Table 4 include the measured values, the predicted values, and the calculated relative error values of the test set. These values were obtained by averaging the output of 50 trained ANNs. The valsartan content of the tablets was also successfully determined without systematic error and with high accuracy. The 1st and 3rd samples exhibit a larger deviation from the measured value. These deviations can be caused by the small input dataset. Despite the two outliers, the average relative error of the method was 3.98 % for the 60 mg target, which is in the range of the ± 5 % limit. Consequently, it can be observed, that despite the vastly wide range of valsartan content in the tablets, the predicted values were never deviated more than a few milligrams from the measured values.

In conclusion, the machine vision method demonstrated the ability to extract relevant information from images containing non-fluorescent API with darker colour, similar to the amlodipine content prediction. The changes observed in the histograms of the G values are associated with the changes in the content of the applied API, resulting in its successful utilization for training a simple ANN model. The smaller particle size of the API and the obtained slight differences in the surface colour were not a limiting factor during the image processing and the prediction. The combination of machine vision and artificial neural networks can offer a versatile solution for the rapid and comprehensive evaluation of various APIs.

The results of the ANN-based API content predictions are compared in Table 5. The relative error values were similar for both a highly and a non-UV fluorescent API. UV imaging proved to be an accurate API content measurement method in the case of two different APIs with different characteristics. However, with the application of extended sample sets the accuracy of the predictions can be further increased.

To place our findings in the literature, the accuracy and other parameters regarding UV imaging and other PAT tools, such as NIR and Raman spectroscopy should be investigated. In a previous paper of the authors (Mészáros et al., 2020), the meloxicam (a coloured API) content of tablets was predicted with a relative error of 4.9 % using single wavelength UV imaging. In the case of both colourless APIs in this work a lower relative error was achieved. Casian et al. (Casian et al., 2017) measured the amlodipine and valsartan content of tablets using NIR and Raman spectroscopy. They reported RMSECV values of 0.48 mg and 2.22 mg with NIR, and 0.44 mg and 1.92 mg with Raman spectroscopy for amlodipine and valsartan respectively. These results are comparable with our RMSE values of 0.112 mg and 2.70 mg. However, there is an enormous difference in investment cost between the spectroscopic

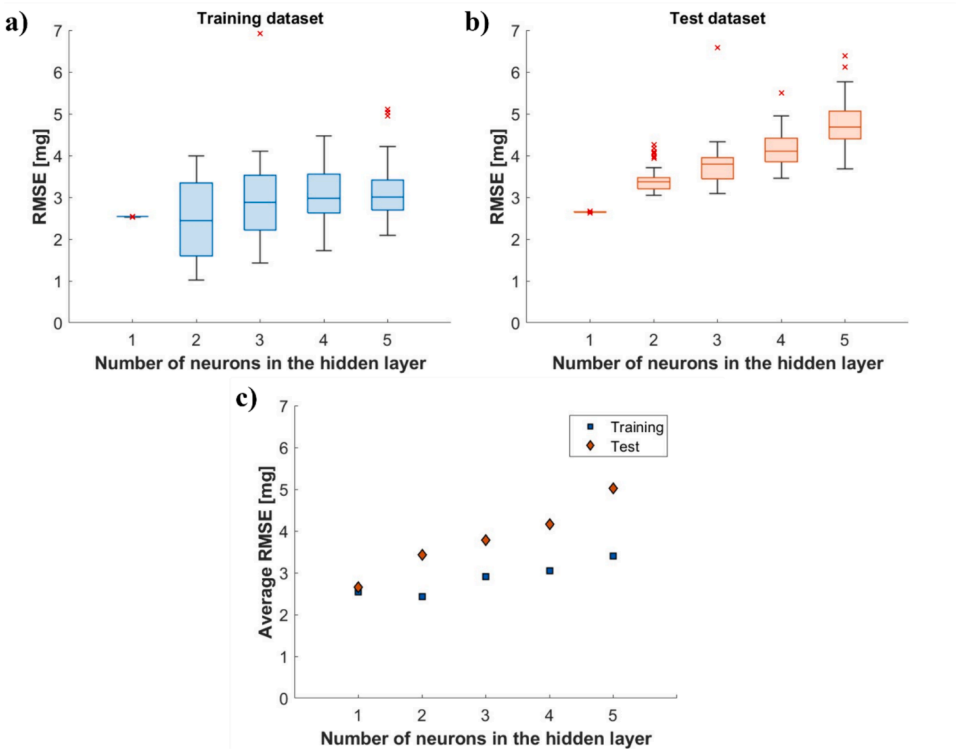

Fig. 9. The results of the optimization process of the ANN-based model for the training (a) and test set (b) of valsartan content prediction with different numbers of neurons in the hidden layer, and the trend obtained in the averaged RMSE values (c).

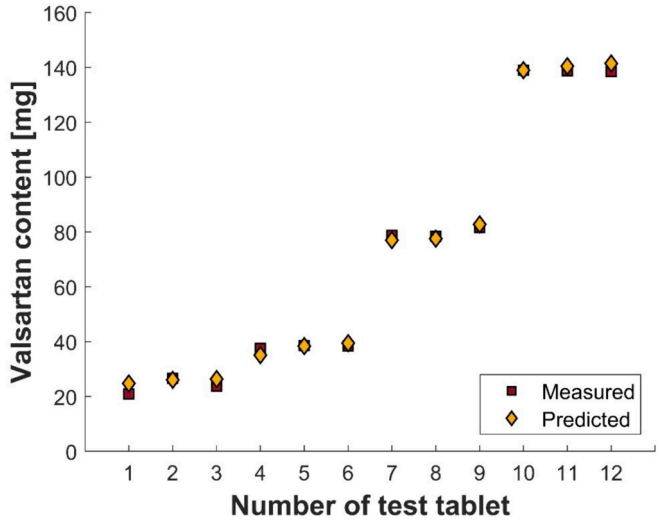

Fig. 10. The valsartan content of the test tablets predicted with the optimized ANN-based model and measured using standard method of UV spectrometry.

methods, where medium level equipment has an asking price of more than 80 000 USD (Hallmark, 2024), and our UV imaging system, with a cost well below a tenth of that, while being more easily implementable by taking up less space and requiring less training for the users. By utilizing imaging techniques, other aspects of the tablets could also be simultaneously inspected, for example their hardness, porosity, disintegration time and the particle size of the API, factors all influencing the dissolution profile of a tablet, which is one of the most important CQAs.

By being a low-cost, fast and non-destructive at-line or off-line system, UV imaging can replace the traditional API content measurement techniques currently practised in the pharmaceutical industry. It is also a huge step in the direction of UV imaging-based in-line, real-time

Table 4
Predicted and measured amlodipine content of the tablets of the test set and the relative error values for each sample.

Number of test tablet [-]	Valsartan content predicted with ANN [mg]	Valsartan content measured with UV spectrometry [mg]	Relative error of prediction [%]
1	24.72	20.92	18.17
2	26.03	26.57	−2.04
3	26.38	23.81	10.78
4	35.10	37.51	−6.43
5	38.41	38.50	−0.24
6	39.43	38.47	2.49
7	77.03	78.76	−2.19
8	77.57	78.40	−1.07
9	82.77	81.64	1.38
10	139.03	138.99	0.03
11	140.46	138.74	1.24
12	141.46	138.48	2.15

Table 5
The comparison of the developed ANN models, according to the selected number of hidden layer neurons and the average relative error of the API content predictions of prepared tablets.

API	Selected number hidden layer neurons [-]	Average relative error of API content prediction [%]
Amlodipine	1	4.41
Valsartan	1	3.98

monitoring, because its measurement time of 50 ms is much quicker compared to previous multispectral UV imaging techniques.

4. Conclusions

This work introduced a novel at-line PAT system, wherein UV imaging is used to predict the API content of tablets containing two colourless APIs, valsartan or amlodipine an order of magnitude faster than what was previously achieved. Artificial neural networks have been applied to determine the API content of the tablets based on the blue and green histograms extracted from UV images. It was found that this machine vision-based method is capable of predicting the amlodipine and valsartan content of tablets with low relative errors. The proposed system has a measurement time of only 50 ms, which enables the at-line analysis of well over 100 tablets per minute. With this simple and cost-effective method, the content uniformity of the tablets could be measured more thorough, while also opening the possibility for the particle size measurement of the API.

The developed method could be used for a vast number of other APIs, making the API content and content uniformity measurements faster and non-destructive for a wide range of pharmaceutical products. This UV imaging-based method could also be augmented in a way to produce a high-throughput in-line API content measurement system, making it possible to investigate all the produced tablets, accomplishing 100 % screening. Other than APIs, excipients can also interact differently with UV illumination, enabling the differentiation of all tablet components, which could be used to create an imaging based chemical mapping method.

CRediT authorship contribution statement

Máté Ficzere: Writing – original draft, Validation, Methodology, Investigation. **Lilla Alexandra Mészáros:** Software, Methodology, Investigation, Data curation. **Anna Diószegi:** Investigation. **Zoltán Bánrévi:** Investigation. **Attila Farkas:** Writing – review & editing, Supervision. **Sándor Lenk:** Investigation. **Dorián László Galata:** Writing – review & editing, Methodology. **Zsombor Kristóf Nagy:** Writing – review & editing, Resources, Funding acquisition, Conceptualization.

Declaration of competing interest

The authors declare that they have no known competing financial interests or personal relationships that could have appeared to influence the work reported in this paper.

Data availability

Data will be made available on request.

Acknowledgements

Project no. RRF-2.3.1-21-2022-00015 has been implemented with the support provided by the European Union. This project was supported by the ÚNKP-23-3-I-BME-23 and ÚNKP-23-5- BME-448 New National Excellence Program of the Ministry of Human Capacities. The project supported by the Doctoral Excellence Fellowship Programme (DCEP) is funded by the National Research Development and Innovation Fund of the Ministry of Culture and Innovation and the Budapest University of Technology and Economics, under a grant agreement with the National Research, Development and Innovation Office. This paper was supported by the János Bolyai Scholarship of the Hungarian Academy of Sciences.

References

Baranwal, Y., Román-Ospino, A.D., Keyvan, G., Ha, J.M., Hong, E.P., Muzzio, F.J., Ramachandran, R., 2019. Prediction of dissolution profiles by non-destructive NIR spectroscopy in bilayer tablets. Int. J. Pharm. 565, 419–436.

Belay, N.F., Busche, S., Manici, V., Shaukat, M., Arndt, S.-O., Schmidt, C., 2021. Evaluation of Transmission Raman spectroscopy and NIR Hyperspectral Imaging for the assessment of content uniformity in solid oral dosage forms☆. Eur. J. Pharm. Sci. 166, 105963.

Butts, M.B., Hoest-Madsen, J., Refsgaard, J.C., 2003. Hydrologic forecasting.

Casian, T., Reznek, A., Vonica-Gligor, A.L., Van Renterghem, J., De Beer, T., Tomuță, I., 2017. Development, validation and comparison of near infrared and Raman spectroscopic methods for fast characterization of tablets with amlodipine and valsartan. Talanta 167, 333–343.

Casian, T., Nagy, B., Kovács, B., Galata, D.L., Hirsch, E., Farkas, A., 2022. Challenges and opportunities of implementing data fusion in process analytical technology—a review. Molecules 27, 4846.

Das, M.K., Chakraborty, T., 2016. ANN in pharmaceutical product and process development, Artificial neural network for drug design, delivery and disposition. Elsevier 277–293.

De Man, A., Uyttersprot, J.-S., Chavez, P.-F., Vandenbroucke, F., Bovart, F., De Beer, T., 2023. The application of Near-Infrared Spatially Resolved Spectroscopy in scope of achieving continuous real-time quality monitoring and control of tablets with challenging dimensions. Int. J. Pharm. 641, 123064.

Djuris, J., Cirin-Varadjan, S., Aleksic, I., Djuris, M., Cvijic, S., Ibric, S., 2021. Application of machine-learning algorithms for better understanding of tableting properties of lactose co-processed with lipid excipients. Pharmaceutics 13, 663.

European Pharmacopoeia Commission, 2019a. Friability of uncoated tablets (2.9.7.), European Pharmacopoeia 10th Edition, pp. 336-337.

European Pharmacopoeia Commission, 2019b. Uniformity of mass of single-dose preparations (2.9.5.), European Pharmacopoeia 10th Edition, pp. 335-336.

Ficzere, M., Mészáros, L.A., Madarász, L., Novák, M., Nagy, Z.K., Galata, D.L., 2021. Indirect monitoring of ultralow dose API content in continuous wet granulation and tableting by machine vision. Int. J. Pharm. 607, 121008.

Food and Drug Administration, 2004. Guidance for industry, PAT-A framework for innovative pharmaceutical development, manufacturing and quality assurance. http://www.fda.gov/cder/guidance/published.html.

Food and Drug Administration, 2024. Drug Recalls, https://www.fda.gov/drugs/drug-safety-and-availability/drug-recalls, accessed: 2024.02.28.

Galata, D.L., Könyves, Z., Nagy, B., Novák, M., Mészáros, L.A., Szabó, E., Farkas, A., Marosi, G., Nagy, Z.K., 2021a. Real-time release testing of dissolution based on surrogate models developed by machine learning algorithms using NIR spectra, compression force and particle size distribution as input data. Int. J. Pharm. 597, 120338.

Galata, D.L., Meszaros, L.A., Ficzere, M., Vass, P., Nagy, B., Szabo, E., Domokos, A., Farkas, A., Csontos, I., Marosi, G., 2021b. Continuous blending monitored and feedback controlled by machine vision-based PAT tool. J. Pharm. Biomed. Anal. 196, 113902.

Galata, D.L., Meszaros, L.A., Kallai-Szabo, N., Szabo, E., Pataki, H., Marosi, G., Nagy, Z. K., 2021c. Applications of machine vision in pharmaceutical technology: A review. Eur. J. Pharm. Sci. 159, 105717.

Hallmark, 2024. Mild Steel Bruker MPA II Multi Purpose NIR Spectrometer, https://www.indiamart.com/proddetail/bruker-mpa-ii-multi-purpose-nir-spectrometer-23359515933.html, accessed: 2024.04.12.

Kandpal, L.M., Tewari, J., Gopinathan, N., Stolee, J., Strong, R., Boulas, P., Cho, B.-K., 2017. Quality assessment of pharmaceutical tablet samples using Fourier transform near infrared spectroscopy and multivariate analysis. Infrared Phys. Technol. 85, 300–306.

Klukkert, M., Wu, J.X., Rantanen, J., Carstensen, J.M., Rades, T., Leopold, C.S., 2016. Multispectral UV imaging for fast and non-destructive quality control of chemical and physical tablet attributes. Eur. J. Pharm. Sci. 90, 85–95.

Mészáros, L.A., Galata, D.L., Madarász, L., Köte, Á., Csorba, K., Dávid, Á.Z., Domokos, A., Szabó, E., Nagy, B., Marosi, G., 2020. Digital UV/VIS imaging: A rapid PAT tool for crushing strength, drug content and particle size distribution determination in tablets. Int. J. Pharm. 578, 119174.

Mészáros, L.A., Farkas, A., Madarász, L., Bicsár, R., Galata, D.L., Nagy, B., Nagy, Z.K., 2022. UV/VIS imaging-based PAT tool for drug particle size inspection in intact tablets supported by pattern recognition neural networks. Int. J. Pharm. 620, 121773.

Nagy, B., Petra, D., Galata, D.L., Démuth, B., Borbás, E., Marosi, G., Nagy, Z.K., Farkas, A., 2019. Application of artificial neural networks for Process Analytical Technology-based dissolution testing. Int. J. Pharm. 567, 118464.

Nagy, B., Galata, D.L., Farkas, A., Nagy, Z.K., 2022. Application of artificial neural networks in the process analytical technology of pharmaceutical manufacturing—a review. AAPS J. 24, 74.

Novikova, A., Carstensen, J.M., Rades, T., Leopold, C.S., 2016. Multispectral UV imaging for surface analysis of MUPS tablets with special focus on the pellet distribution. Int. J. Pharm. 515, 374–383.

Peeters, M., Peeters, E., Van Hauwermeiren, D., Cogoni, G., Liu, Y., De Beer, T., 2022. Determination and understanding of lead-lag between in-line NIR tablet press feed frame and off-line NIR tablet measurements. Int. J. Pharm. 611, 121328.

Péterfi, O., Nagy, Z.K., Sipos, E., Galata, D.L., 2023. Artificial intelligence-based prediction of in vitro dissolution profile of immediate release tablets with near-infrared and Raman spectroscopy. Period. Polytech. Chem. Eng. 67, 18–30.

Rossi, C.V., 2022. A comparative investment analysis of batch versus continuous pharmaceutical manufacturing technologies. J. Pharm. Innov. 17, 1373–1391.

Sandoz Group, A.G., 2018. Valsartan Sandoz - Package leaflet: Information for the patient, https://docetp.mpa.se/LMF/Valsartan%20Sandoz%20film-coated%20tablet%20ENG%20PL_09001bee807a7171.pdf, accessed: 2024.04.08.

Teva, 2022. Amlodipine Teva - Package leaflet: Information for the user, https://www.hpra.ie/img/uploaded/swedocuments/8aaf5eef-e387-4f53-9f16-bbbea875cd5b.pdf, accessed: 2024.04.08.

Wagner, K.G., Krumme, M., Schmidt, P.C., 1999. Investigation of the pellet-distribution in single tablets via image analysis. Eur. J. Pharm. Biopharm. 47, 79–85.

Wagner, K.G., Krumme, M., Beckert, T.E., Schmidt, P.C., 2000. Development of disintegrating multiple-unit tablets on a high-speed rotary tablet press. Eur. J. Pharm. Biopharm. 50, 285–292.

Wang, X., Mao, D.-Z., Yang, Y.-J., 2021. Calibration transfer between modelled and commercial pharmaceutical tablet for API quantification using backscattering NIR, Raman and transmission Raman spectroscopy (TRS). J. Pharm. Biomed. Anal. 194, 113766.

Wu, J.X., Rehder, S., van den Berg, F., Amigo, J.M., Carstensen, J.M., Rades, T., Leopold, C.S., Rantanen, J., 2014. Chemical imaging and solid state analysis at compact surfaces using UV imaging. Int. J. Pharm. 477, 527–535.

Yu, L.X., 2008. Pharmaceutical quality by design: product and process development, understanding, and control. Pharm. Res. 25, 781–791.